Fractal Dimension of Mucoadhesive Polymer Hyaluronan for Pharmaceutical Formulations

Francisco Torrens*,[1] and Gloria Castellano[2]

[1]Institut Universitari de Ciència Molecular, Universitat de València, Edifici d'Instituts de Paterna, P. O. Box 22085, E-46071 València, Spain

[2]Cátedra Energesis de Tecnología Interdisciplinar, Universidad Católica de Valencia *San Vicente Mártir*, Guillem de Castro 94, E-46001, València, Spain

Mucoadhesive polymers are used in pharmaceutical formulations to release drugs in mucosal areas, *e.g.*, gastrointestinal/vaginal tracts, ocular mucosa and bucal/nasal cavity. They interact and become fixed to mucus *via* mechanisms, *e.g.*, molecular interpenetration, van der Waals forces, hydrophobic interactions, electrostatic forces, H-bonds, *etc.*, which increase organism residence period and drug bioavailability. Drugs and polymers physicochemical properties, *e.g.*, molecular weight, ionization, concentration, polymer swelling kinetics, *etc.*, affect formulation mucoadhesion, rheological behaviour and drug absorption. Fractal dimension was examined for transdermal-delivery drug models. The method is extended to polymers. Hyaluronan (HA) is selected as mucoadhesive and biodegradable polymer. Geometric, topological and fractal analyses are carried out with program TOPO. Reference calculations are performed with algorithm GEPOL. The TOPO underestimate molecular volume and surface area by 0.7% and 5%, respectively. Molecular globularity is overestimated by 5% and rugosity, underestimated by 5%. Sovent-accessible surface is undercalculated by 3%: when going from hexamer HA^{3-} to HA·3Ca to HA·3Ca·9H_2O, the hydrophobic term increases by 42% and decays by 26%; the hydrophilic part drops by 14% and rises by 58%. Fractal dimension of HA results 1.566. On going to HA·3Ca to HA·3Ca·9H_2O, it increases by 2% and 1%. Fractal dimension of external atoms augments by 11%. In particular, for HA it results 1.725. When going to HA·3Ca to HA·3Ca·9H_2O, it increases by 4% and 0.3%.

Key words: *fractal dimension, drug absorption, drug delivery, mucoadhesive polymer, mucosa, metal hyaluronate*

INTRODUCTION

Hyaluronic acid (HA) is a high molecular weight polysaccharide present in the extracellular matrix of most vertebrate tissues [1]. Its functions vary from maintaining the constant volume of interstitial fluid to organizing extracellular matrix and various immunosuppressive functions [2]. Presence of HA on plasma membranes and concentration variation in pericellular spaces are associated with cell aggregation during morphogenesis, and metastasis formation during malignant transformation and tumours invasion [3–5]. The HA is a polymer composed of linear repeats of disaccharide unit containing 2-acetamido-2-deoxy-D-glucosamine (NAG)/D-glucuronic acid (GCU), linked by (1→3/4) glycosidic bonds (*cf.* Fig. 1). A typical HA molecule consists of 10^4 NAG/GCU units. The overall anionic charge of an HA molecule under physiological conditions is caused by repeating NAG/GCU units containing sites COO^-, which interaction with metal cations is important contributing to the overall supermolecular structure of HA [6]. Other factors include: counterion type, p*H*, temperature and hydration extent, with the former being most important [7,8]. Structural/literature data for transition metal complexes with HA remain scarce/limited to co-ordination complexes in aqueous solution with Ca^{2+}, Ag^{+}, Cd^{2+}, Pb^{2+} and Fe^{3+} [9–11]. In the past, X-ray fibre diffraction was successfully used to solve solid-state structure of HA, containing various cations from the first/second groups of periodic table, where 2/4-fold-helices formation was reported [12–15]. Polyanion conformation is stabilized by H-bonds across glycosidic linkages between HA monomers. Adjacent antiparallel chains are held together *via* $–COO^–Ca^{2+}–^–OOC–$ bridges and six H-bonded water molecules. It was suggested that polymer secondary structure will be similar to Ca^{2+} HA in cases of other divalent cations. Amorphous divalent metal HA containing Cu^{2+}, Ni^{2+}, Mn^{2+} or Co^{2+} were prepared at p*H* 5.5 by precipitation from aqueous solutions with cold ethanol. Local structure around $metal^{2+}$ was determined by extended X-ray absorption fine structure (EXAFS)/X-ray absorption near edge structure (XANES) [16,17]. Co-ordination polyhedron around Cu^{2+} is distorted octahedron. Four O atoms at average distance of 1.95Å occupy

planar equatorial sites. At axial sites, O atoms are present at 2.46Å. Though O atoms are preferred at axial positions, N atoms from NAG cannot be excluded.

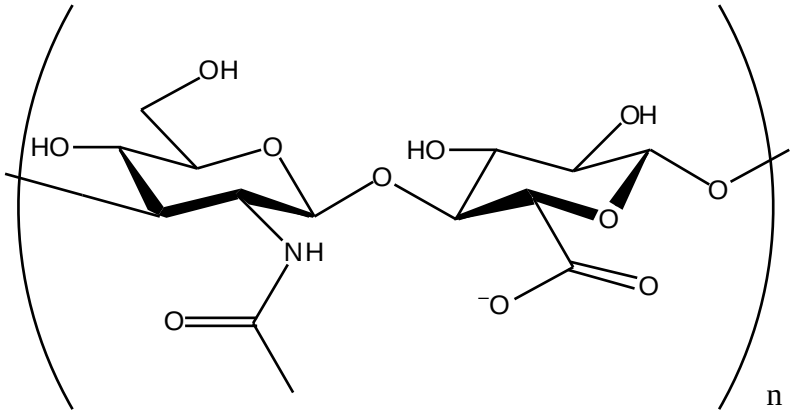

Fig. 1. Disaccharide repeating unit of HA comprising NAG/GCU. The M_w lies in 10^4–10^7 g·mol^{-1}.

Using quantum chemical methods, basic NAG/GCU unit of HA was studied. Semiempirical molecular orbital (MO) methods and *ab initio* calculations showed good agreement between optimized geometries and available crystallographic data [18]. Synthesized Ca^{2+}/Cu^{2+} HA are amorphous materials making analysis difficult, as X-ray diffraction patterns cannot be used to explain experimental EXAFS data. One possible way is to use a combined quantum mechanical/molecular mechanics (QM/MM) approach [19], which was successfully used in computational enzymology and employed in studies of metal cation binding to protein/HA [20–22]. Transition-metal binding was studied using density-functional theory (DFT) methods [23–27]. In all cases, atomistic simulations proved to be an invaluable tool for elucidation of experimental structural data. Larger systems can be studied using QM/MM. While the approach was successfully used in computational enzymology, it was also employed in studies of metal cation binding to protein/HA [28–33]. In the latter, QM/MM proved to be an invaluable tool for elucidation of experimental structural data. A QM/MM calculation of HA complexation with Ca^{2+}/Cu^{2+} was performed [34].

Mucoadhesive polymers are used in pharmaceutical formulations to release drugs in mucosal areas, *e.g.*, gastrointestinal/vaginal tracts, ocular mucosa and buc/nasal cavity [35]. They interact/become fixed to mucus *via* mechanisms: molecular interpenetration, van der Waals forces, hydrophobic interactions, electrostatic forces, H-bonds, *etc.*, which increase organism residence

period/drug bioavailability [36–39]. Drugs/polymers physicochemical properties: molecular weight, ionization, concentration, polymer swelling kinetics, *etc.*, affect formulation mucoadhesion, rheological behaviour and drug absorption [40]. In the present report, the method is extended to polymers. The model uses program TOPO to perform HA geometric, topological and fractal analyses. In earlier publications, TOPO was applied to calculation of fractal dimension of molecules, *e.g.*, percutaneous enhancers phenyl alcohols [41]/4-alkylanilines [42]. The aim of this report is to find properties that distinguish HA, Ha·3Ca and HA·3Ca·9H_2O. The goal of this study is index usefulness validation *via* capability to differentiate HAs.

RESULTS AND DISCUSSION

The HA was selected as mucoadhesive and biodegradable polymer. A comparative analysis of $Ca_3(C_{14}H_{20}O_{11}N)_3 \cdot 9H_2O$ was carried out in three HA forms: hexamer HA^{3-}, Ha·3Ca and HA·3Ca·9H_2O (Protein Data Bank code 4HYA, *cf.* Fig. 2). The HA consists of six saccharide residues (126 atoms) and presents a molecular weight M_w = 1123g·mol^{-1}. There are three Ca^{2+} and nine H_2O molecules around the glycosaminoglycan hexamer.

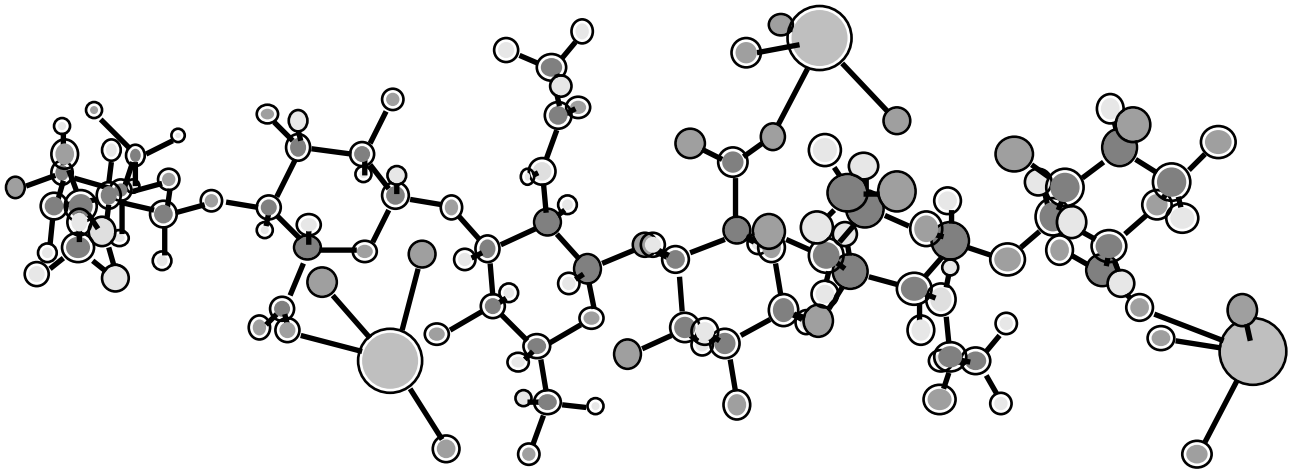

Fig. 2. Hydrogen-suppressed structure of hyaluronic acid hexamer Ha·3Ca·9H_2O.

Geometric and topological analyses were carried out with our program TOPO (*cf.* Table 1). Reference calculations were performed with our version of algorithm GEPOL. Software TOPO underestimated molecular volume V and surface area S by 0.7% and 5%, respectively. Topological

index molecular globularity *G* resulted overestimated by 5% and rugosity *G'* was underestimated by 5%.

Table 1. Geometric descriptors and topological indices of hyaluronic acid (HA).

Molecule	***V*[a]**	***V* Ref.[b]**	***S*[c]**	***S* Ref.[b]**	***G*[d]**	***G* Ref.[b]**	***G'*[e]**	***G'* Ref.[b]**
HA^{3-}	816.4	822.8	942.78	999.24	0.448	0.425	1.155	1.214
HA·3Ca	913.3	919.9	1069.45	1128.66	0.426	0.405	1.171	1.227
$HA{\cdot}3Ca{\cdot}9H_2O$	1070.0	1077.8	1247.91	1320.73	0.405	0.385	1.166	1.225

[a] Molecular volume ($Å^3$).

[b] Reference calculation carried out with program GEPOL.

[c] Molecular surface area ($Å^2$).

[d] Molecular globularity.

[e] Molecular rugosity ($Å^{-1}$).

Water solvent-accessible surface analysis was carried out (*cf.* Table 2). Sovent-accessible surface (AS) area was underestimated by 3%. When going from hexamer HA^{3-} to HA·3Ca to $HA{\cdot}3Ca{\cdot}9H_2O$, the hydrophobic solvent-accessible surface (HBAS) area increased by 42% and decayed by 26%, respectively; the hydrophilic solvent-accessible surface (HLAS) area decayed by 14% and increased by 58%. The HLAS resulted the geometric descriptor most sensitive to the presence of Ca^{2+} and, especially, H_2O. The fractal dimension *D* of HA turned out to be 1.566. On going to HA·3Ca to $HA{\cdot}3Ca{\cdot}9H_2O$, *D* increased by 2% and 1%. The *D* resulted somewhat sensitive to the occurrence of Ca^{2+} and H_2O. The fractal dimension averaged for non-buried atoms *D'* increased, in general, by 11% with regard to *D*. In particular, *D'* of HA resulted 1.725. When going to HA·3Ca to $HA{\cdot}3Ca{\cdot}9H_2O$, it augmented by 4% and 0.3%. The *D'* resulted greatly sensitive to the incidence of Ca^{2+} and H_2O.

Table 2. Geometric descriptors and fractal dimensions of the solvent-accessible surface of HA.

Molecule	**AS[a]**	**AS Ref.[b]**	**HBAS[c]**	**HLAS[d]**	***D*[e]**	***D'*[f]**

HA^{3-}	1255.03	1293.95	589.72	665.31	1.566	1.725
HA·3Ca	1409.77	1453.85	834.57	575.20	1.601	1.792
$HA·3Ca·9H_2O$	1530.07	1578.40	620.88	909.19	1.625	1.798

[a] Water solvent-accessible surface area ($Å^2$).

[b] Reference calculation carried out with program GEPOL.

[c] Hydrophobic solvent-accessible surface area ($Å^2$).

[d] Hydrophilic solvent-accessible surface area ($Å^2$).

[e] Molecular fractal dimension.

[f] Molecular fractal dimension averaged for non-buried atoms.

EXPERIMENTAL

In our program TOPO for the theoretical simulation of the shape of crystal fragments [43], their surface is represented by the external surface of a set of overlapping spheres with appropriate radii, centred on the atomic nuclei [44]. The fragment is treated as a solid in space, defined by tracing spheres about the atomic nuclei. It is computationally enclosed in a graduated rectangular box, and the geometric descriptors, evaluated by counting points within the solid or close to chosen surfaces. They can be calculated the fragment volume *V,* surface area *S* and two topological indices of fragment shape. Consider S_e as the surface area of a sphere whose volume is equal to the fragment volume *V* [45]. The ratio $G = S_e/S$ is interpreted as a descriptor of fragment globularity. The ratio $G' = S/V$ is interpreted as a descriptor of fragment *rugosity.*

The properties of the systems solvated in water are strongly related to the contact surface between solute and water molecules. Starting from this fact, another molecular geometric descriptor was proposed: the *solvent-accessible surface* area AS [46]. The AS is defined by means of a probe sphere, which is allowed to roll on the outside while maintaining contact with the *bare* molecular surface [47]. The AS can be calculated in the same way as the bare molecular surface area by means of pseudoatoms, whose van der Waals radii [48] have been increased by the probe radius *R* [49]. The *accessibility* is a dimensionless quantity varying between 0 and 1, as well as represents the

ratio of the solvent-accessible surface area in a particular structure to the solvent-accessible surface area of the same atom when isolated from the molecule. The *fractal dimension D* of the molecules may be obtained as $D = 2 - d(\log AS)/d(\log R)$ [50]. The fractal dimension D provides a quantitative indication of the degree of surface accessibility toward different solvents [51]. Program TOPO allows an atom-to-atom analysis of D on each atom i, to obtain an atomic dimension index D_i from the atomic contributions to the accessible surface area AS_i. The D_i can be weight averaged to obtain a new molecular dimension index $D' = (\Sigma_i AS_i D_i)/AS$, where the AS_i are used as weights for the D_i. Notice that if an $AS_i = 0$ for any probe, D_i cannot be calculated for atom i and, so, this atom does not contribute to D'. Thus, D' represents a D averaged for atoms *nonburied* (accessible) to any of the solvent-accessible surfaces in the range of probe spheres. In particular, $D' = D$ for systems without buried atoms, *e.g.*, inert gases, fullerenes, *etc.*

A version of TOPO was implemented in our versions of programs AMYR [52], GEPOL [53] and SURMO2 [54]. Program AMYR carries out the theoretical simulation of molecular associations and chemical reactions. Software GEPOL performs an accurate triangular tessellation of the molecular surface and is used for reference calculations. Both TOPO and GEPOL recognize the cavities in inclusion molecules and are adequate to study intercalation compounds. On the other hand, SURMO2 does not recognize cavities. Furthermore, the combination of SURMO2 and GEPOL results allows the characterization of the molecular surface of internal cavities. Our version of SURMO2 was corrected for the deviation from the spherical shape, by dividing each point contribution by the cosine of the angle formed by the semiaxis and the corresponding normal vector to the surface at this point. The volume and surfaces of crystal fragments with cavities have been corrected by maximizing, in each angular orientation, the distance of the most distant atom in each semiaxis.

CONCLUSONS

From the present results and discussion the following conclusions can be drawn.

1. The hydrophilic solvent-accesible surface area resulted the geometric descriptor most sensitive to the presence of Ca^{2+} and H_2O.

2. On going to hyaluronan·3Ca/·9H$_2$O, the fractal dimension of hyaluronan (1.566) increased by 2% and 1%, respectively. The fractal dimension of non-buried atoms (1.725) augmented by 4% and 0.3%. It resulted greatly sensitive to the occurrence of Ca^{2+} and, especially, H_2O.

3. The fractal dimension of external atoms increased by 11% with regard to the fractal dimension.

4. Hyaluronan is an important component of articular cartilage, where it is present as a coat around each chondrocyte. When aggrecan monomers bind to hyaluronan in the presence of link protein, large, highly anionic aggregates form, which imbibe water and are responsible for cartilage resistance to compression. The molecular weight of hyaluronan in cartilage decays with age but the amount increases.

5. Polymer rheological behaviour formulated in pH 4–7 did not differ, which is proper of unstructured systems. The pH < 4 generated gels because of hydrophobic interactions/H-bonds; gels resulted promising for administration on skin/mucous membranes. Interest exists in hyaluronan addition into gels to improve mucoadhesive properties.

ACKNOWLEDGEMENTS

One of the authors, F. T., acknowledges financial support from the Spanish Ministerio de Ciencia e Innovación (Project No. BFU2010–19118).

REFERENCES

[1] Balazs, E.A., Ed. *The Chemistry and Molecular Biology of the Intercellular Matrix*; Academic: New York, NY, 1970.

[2] Alberts, B.; Johnson, A.; Lewis, J.; Raff, M.; Roberts, K.; Walter, P. *Molecular Biology of the Cell*; Garland, New York, NY, 2002.

[3] Laurent, T.C.; Fraser, J.R.E. Hyaluronan, *FASEB J.* **1992**, *6*, 2397–2404.

[4] Goa, K.L.; Benfield, P.; Hyalurinic-acid – A review of its pharmacology and use as a surgical aid in ophthalmology, and its therapeutic potential in joint disease and wound-healing. *Drugs* **1994**, *47*, 536–566.

[5] Zimmerman, E.; Geiger, B.; Addadi, L. Initial stages of cell-matrix adhesion can be mediated and modulated by cell-surface hyaluronan. *Biophys. J.* **2002**, *82*, 1848–1857.

[6] Moulabbi, M.; Broch, H.; Rober, L.; Vasilescu, D. Quantum molecular modeling of hyaluronan. *J. Mol. Struct. (THEOCHEM)* **1997**, *395*, 477–508.

[7] Sipos, P.; Veber, M.; Burger, K.; Illes, J.; Machula, G. Hyaluronate–metal ion interactions: Correlations between viscosimetric, potentiometric, polarographic and electrophoretic data. *Acta Chim. Hung. Models Chem*. **1992**, *129*, 671–683.

[8] Morris, E.R.; Rees, D.A.; Welsh, E.J. Conformation and dynamic interactions in hyaluronate solutions. *J. Mol. Biol*. **1980**, *138*, 383–400.

[9] Figueroa, N.; Nagy, B.; Chakrabarti, B. Cu^{2+}–hyaluronic acid complex-spectrophotometric detection. *Biochem. Biophys. Res. Commun*. **1977**, *74*, 460–465.

[10] Sterk, H.; Braun, M.; Schmut, O.; Feichtinger, H. Investigation of the hyaluronic acid–copper complex by N.M.R. spectroscopy. *Carbohydr. Res.* **1985**, *145*, 1–11.

[11] Lapcik, L.; Dammer, C.; Valko, M. Hyaluronic acid–copper(ii) complexes-spectroscopic characterization. *Colloid Polym. Sci.* **1992**, *201*, 1049–1052.

[12] Sheehan, J.K.; Atkins, E.D.; X-ray fiber diffraction study of conformational-changes in hyaluronate induced ni the presence of sodium, potassium and calcium cations. *Int. J. Biol. Macromol*. **1983**, *5*, 215–221.

[13] Atkins, E.D.; Sheehan, J.K.; Phelps, C.F. Conformation of mucopolysaccharides-hyaluronates. *Biochem. J.* **1972**, *128*, 1255–1263.

[14] Mitra, A.K.; Raghunathan, S; Sheehan, J.K.; Arnott, S. Hyaluronic-acid-molecular-conformations and interactions in the orthorhombic and tetragonal forms containing sinuous chains. *J. Mol. Biol*. **1983**, *169*, 829–859.

[15] Winter, W.T.; Arnott, S. Hyaluronic acid: The role of divalent cations in conformation and packing. *J. Mol. Biol*. **1977**, *117*, 761–784.

[16] Tratar Pirc, E.; Arcon, I.; Bukovec, P.; Kodre, A. Preparation and characterisation of copper(II) hyaluronate. *Carbohydr. Res.* **2000**, *324*, 275–282.

[17] Tratar Pirc, E.; Arcon, I.; Kodre, A.; Bukovec, P. Metal-ion environment in solid Mn(II), Co(II) and Ni(II) hyaluronates. *Carbohydr. Res.* **2004**, *339*, 2549–2554.

[18] Eklund, R.; Widmalm, G.; Molecular dynamics simulations of an oligosaccharide using a force field modified for carbohydrates. *Carbohydr. Res.* **2003**, *338*, 393–398.

[19] Warshel, A., Levitt, M. Theoretical studies of enzymic reactions: Dielectric, electrostatic and steric stabilization of the carbonium ion in the reaction of lysozyme. *J. Mol. Biol*. **1976**, *103*, 227–249.

[20] Masgrau, L.; Roujeinikova, A.; Johannissen, L.O.; Hothi, P.; Basran, J.; Ranaghan, K.E.; Mulholland, A.J.; Sutcliffe, M.J.; Scrutton, N.S.; Leys, D.; Atomic description of an enzyme reaction dominated by proton tunneling. *Science* **2006**, *312*, 237–241.

[21] Zidar, J.; Tratar Pirc, E.; Hodoscek, M.; Bukonec, P. Copper(II) ion binding to cellular prion protein. *J, Chem. Model.* **2008**, *48*, 283–287.

[22] Tratar Pirc, E.; Zidar, J., Bukovec, P.; Hodoscek, M. Molecular modeling of cobalt(II) hyaluronate. *Carbohydr. Res.* **2005**, *340*, 2064–2069.

[23] Hofstetter, T.E.; Howder, C.; Berden, G.; Oomens, J.; Armentrout, P.B. Structural elucitation of biological and toxicological complexes: Investigation of monomeric and dimeric complexes of histidine with multiply charged transition metal (Zn and Cd) cations using IR action spectroscopy. *J. Phys. Chem. B* **2011**, *115*, 12648–12661.

[24] Remko, M.; Fitz, D.; Broer, R.; Rode, B.M. Effect of metal ions (Ni^{2+}, Cu^{2+} and Zn^{2+}) and water coordination on the structure of L-phenylalanine, L-tyrosine, L-tryptophan and their zwitterionic forms. *J. Mol. Model.* **2011**, *17*, 3117–3128.

[25] Khodabandeh, M.H.; Hamid, R.; Zare, K., Zahedi, M. A theoretical elucidation of coordination properties of histidine and lysine to Mn^{2+}. *Int. J. Mass Spectrom.* **2012**, *313*, 47–57.

[26] Siegbahn, P.E.; The performance of hybrid DFT for mechanisms involving transition metal complexes in enzymes. *J. Biol. Inorg. Chem*. **2006**, *11*, 695–701.

[27] Minenkov, Y.; Singstad, Å. Occhipinti, G.; Jensen, V.R.; The accuracy of DFT-optimized geometries of functional transition metal compounds: A validation study of catalysts for olefin metathesis and other reactions in the homogeneous phase. *Dalton Trans*. **2012**, *41*, 5526–5541.

[28] Becke, A.D. Density-functional exchange-energy approximation with correct asymptotic-behavior. *Phys. Rev. A* **1988**, *38*, 3098–3100.

[29] Lee, C.T.; Yang, W.T.; Parr, G. Development of the Colle-Salvetti correlation-energy formula into a functional of the electron-density. *Phys. Rev. B* **1988**, *37*, 785–789.

[30] Zhao, Y.; Truhlar, D. The M06 suite of density functionals for main group thermochemistry, thermochemical kinetics, noncovalent interactions, excited states, and transition elements: Two new functionals and systematic testing of four M06-class functionals and 12 other functional. *Theor. Chem. Acc*. **2008**, *120*, 215–241.

[31] MacKerell, A.D., Jr.; Bashford, D.; Bellott, M.; Dunbrack, R.L., Jr.; Evanseck, J.D.; Field, M.J.; Fischer, S.; Gao, J.; Guo, H.; Ha, S.; Joseph-McCarthy, D.; Kuchnir, L.; Kuczera, K.; Lau, F.T.K.; Mattos, C.; Michnick, S.; Ngo, T.; Nguyen, D.T.; Prodhom, B.; Reiher, W.E., III, Roux, B.; Schlenkrich, M.; Smith, J.C.; Stote, R.; Straub, J.; Watanabe, M.; Wiórkiewicz-Kuczera, J.; Yin, D.; Karplus, M. All-atom empirical potential for molecular modeling and dynamics studies of proteins. *J. Phys. Chem. B* **1998**, *102*, 3586–3616.

[32] Brooks, B.R.; Bruccoleri, R.E.; Olafson, B.D.; States, D.J.; Swaminatham, S.; Karplus, M. CHARMM: A program for macromolecular energy, minimization, and dynamics calculations. *J. Comput. Chem*. **1983**, *4*, 187–217.

[33] Brooks, B.R.; Brooks, C.L., III; Mackerell, A.D., Jr.; Nilsson, L.; Petrella, R.J.; Roux, B.; Won, Y.; Archontis, G.; Bartels, C.; Boresch, S.; Caflisch, A.; Caves, L.; Cui, Q.; Dinner, A.R.; Feig, M.; Fischer, M.; Gao, J.; Hodoscek, M.; Im, W.; Kuczera, K.; Lazaridis, T.; Ma, J.; Ovchinnikov, V.; Paci1, E.; Pastor, R.W.; Post, C.B.; Pu, J.Z.; Schaefer, M.; Tidor, B.; Venable, R.M.; Woodcock, H.L.; Wu, X.; Yang, W.; York, D.M.; Karplus, M. CHARMM: The biomolecular simulation program. *J. Comput. Chem*. **2009**, *30*, 1545–1614.

[34] Tratar Pirc, E.; Zidar J.; Bukovec, P. A computational study of calcium(II) and copper(II) ion binding to the hyaluronate molecule. *Int. J. Mol. Sci.* **2012**, *13*, 12036–12045.

[35] Asane, G.S.; Nirmal, S.A.; Rasal, K.B.; Naik, A.A.; Mahadik, M.S.; Rao, Y.M. Polymers for mucoadhesive drug delivery system: Current status. *Drug Dev. Ind. Pharm*. **2008**, *34*, 1246–1266.

[36] Peppas, N.A.; Buri, P.A. Surface, interfacial and molecular aspects of bioadhesion on soft tissues. *J. Control Release* **1985**, *2*, 257–275.

[37] Gu, J.M.; Robinson, J.R.; Leung, S.H. Binding of acrylic polymers to mucin/epithelial surfaces: Structure–property relationships. *Crit. Rev. Ther. Drug Carrier Syst.* **1988**, *5*, 21–67.

[38] Woodley, J. Bioadhesion: New possibilities for drug administration? *Clin. Pharmacokinet.* **2001**, *40*, 77–84.

[39] Smart, J.D. The basics and underlying mechanisms of mucoadhesion. *Adv. Drug Deliv. Rev*. **2005**, *57*, 1556–1568.

[40] Pliszczak, D.; Bordes, C.; Bourgeois, S.; Marote, P.; Zahouani, H, Tupin, S.; Pailler Mattei, C.; Lantéri, P. Mucoadhesion evaluation of polysaccharide gels for vaginal application by using rheological and indentation measurements. *Colloids Surf., B* **2012**, *92*, 168–174.

[41] Torrens, F. Fractal dimension of transdermal-delivery drug models. *Leb. Sci. J.* **2004**, *5*(1), 61–70.

[42] Torrens, F.; Castellano, G. Fractal dimension of transdermal-delivery drug models: 4-Alkylanilines. *J. Liq. Chromatogr. Relat. Technol.* **2008**, *31*, 2337–2347.

[43] Torrens, F.; Ortí, E.; Sánchez-Marín, E. Vectorized TOPO program for the theoretical simulation of molecular shape. *J. Chim. Phys. Phys.-Chim. Biol*. **1991**, *88*, 2435–2441.

[44] Meyer, A.Y. Molecular mechanics and molecular shape. Part 1. Van der Waals descriptors of simple molecules. *J. Chem. Soc., Perkin Trans. 2* **1985**, 1161–1169.

[45] Meyer, A.Y. Molecular mechanics and molecular shape. V. On the computation of the bare surface area of molecules. *J. Comput. Chem*. **1988**, *9*, 18–24.

[46] Lee, B.; Richards, F.M. The interpretation of protein structures: Estimation of static accessibility. *J. Mol. Biol*. **1971**, *55*, 379–400.

[47] Hermann, R.B. Theory of hydrophobic bonding. II. The correlation of hydrocarbon solubility in water with solvent cavity surface area. *J. Phys. Chem*. **1972**, *76*, 2754–2759.

[48] Bondi, A. Van der Waals volumes and radii. *J. Phys. Chem*. **1964**, *68*, 441-451.

[49] Wodak, S.J.; Janin, J. Analytical approximation to the accessible surface area of proteins. *Proc. Natl. Acad. Sci. U.S.A*. **1980**, *77*, 1736–1740.

[50] Lewis, M.; Rees, D.C. Fractal surfaces of proteins. *Science* **1985**, *230*, 1163–1165.

[51] Torrens, F.; Sánchez-Marín, J.; Nebot-Gil, I. New dimension indices for the characterization of the solvent-accessible surface. *J. Comput. Chem*. **2001**, *22*, 477–487.

[52] Torrens, F.; Rubio, M.; Sánchez-Marín, J. AMYR 2: A new version of a computer program for pair potential calculation of molecular associations. *Comput. Phys. Commun*. **1998**, *115*, 87–89.

[53] Pascual-Ahuir, J.L.; Silla, E.; Tomasi, J.; Bonaccorsi, R. Electrostatic interaction of a solute with a continuum. Improved description of the cavity and of the surface cavity bound charge distribution. *J. Comput. Chem*. **1987**, *8*, 778–787.

[54] Terryn, B.; Barriol, J. On the evaluation of the usual quantities or coefficients related to the shape of a molecule approximated on the basis of the van der Waals radii. *J. Chim. Phys. Phys.-Chim. Biol*. **1981**, *78*, 207–212.